Quasiperiodic patterns in Rayleigh-Bénard convection under gravity modulation

Ulrike E. Volmar and Hanns Walter Müller
Institut für Theoretische Physik, Universität des Saarlandes, D-66041 Saarbrücken, Germany
(Received 24 April 1997)

We investigate nonlinear three-dimensional convection under gravity modulation. Depending upon modulation frequency and amplitude, unstable modes in harmonic or subharmonic temporal resonance with the mechanical drive can be observed. We focus on a situation where both modes compete. In non-Boussinesq fluids the dominating interaction mechanism is a nonlinear triad wave-vector resonance. We construct a minimum Galerkin model which describes the competition between several regular convection patterns. Our results indicate that squares or quasiperiodic patterns with a 12-fold rotational axis are the preferred convection structures. [S1063-651X(97)00911-2]

PACS number(s): 47.54.+r, 47.27.Te, 47.20.Ky

I. INTRODUCTION

Thermal convection under temporal modulation of the control parameter gives rise to new linear and nonlinear properties compared to the classical unmodulated Rayleigh-Bénard convection [1]. On the linear level the critical Rayleigh number R_c and the critical wave number k_c for the onset of modulated convection were investigated [2–5]. It is well known [3] that a fluid layer heated from above can be destabilized if the mechanical vibration is sufficiently strong. Unstable modes in either synchronous or subharmonic resonance with the external modulation appear. Under special circumstances bicritical situations occur, in which a harmonic and a subharmonic mode become unstable at the same Rayleigh number but at different wave numbers.

On the nonlinear level two principal methods of investigation have been proven to be useful. The Galerkin technique expands the spatial dependence of the hydrodynamic field in an appropriate set of test functions, and thus reduces the partial field equations to ordinary differential equations. By considering only a few Galerkin modes analytical progress can be made [5,6], otherwise fully developed two- or three-dimensional convection can be treated by computer simulations [7–9]. The alternative method derives amplitude equations by a systematic perturbation expansion around the conductive state. These equations describe the slow temporal and spatial dynamics of the critical convection mode and are useful to predict patterns and secondary instabilities or transitions [10,11]. We also mention a number of experiments, dealing either with the onset of the instability [12–14] or with nonlinear pattern formation [15,16].

In the present paper we concentrate on pattern formation close to bicritical situations, where a subharmonic and a harmonic instability mode compete. This point has not received any attention in the past. By virtue of the interplay between two different length scales we expect the occurrence of new nontrivial convective structures. Our investigation is motivated by the observation of a quasiperiodic pattern in the Faraday instability [17], when operated close to a bicritical instability. These structures can be pictured as two sets of hexagons superimposed onto each other, giving a 12-fold rotational symmetry. As this invariance is incompatible with the translational order of a periodic tiling, these patterns are denoted as quasiperiodic.

In systems with quadratic nonlinearities showing two-dimensional patterns, the generic nonlinear interaction is a three-wave-vector resonance. In a monocritical situation, where *one* circle of critical wave numbers is unstable [18], this mechanism is known to force hexagonal patterns [19–21] close above the onset of the instability. This argument applies for Rayleigh-Bénard convection in non-Oberbeck-Boussinesq (NOB) fluids. In OB fluids the up-down symmetry of the system prohibits the triad wave-vector resonance and instead convective motion in the form of rolls occurs [20,21]. In the present paper we want to take advantage of the three-wave-vector coupling and thus introduce non-OB effects as a weak perturbation. Our aim is to generalize the triad interaction for bicritical situations and to show how this mechanism can be used to force complicated convection structures.

The method of investigation is a multimode Galerkin technique, which gives sufficient complexity to allow the competition between roll, square, hexagonal, and quasiperiodic structures. After introducing the system and establishing the basic evolution equations in Sec. II, we perform a linear analysis (Sec. III) to get a complete view over the stability chart, and the bicritical points. A previously published paper [8] appears to be incomplete as important stability branches are missing. In Sec. IV we proceed to the nonlinear part and discuss in greater detail the three-wave-vector resonance, when applied to bicritical situations. To achieve our objective we have to release the OB approximation and introduce a weakly temperature-dependent viscosity. A model system of 25 ordinary differential equations is obtained by invoking the Galerkin technique (Sec. V). These equations are solved by numerical integration. Besides square patterns we also observe quasiperiodic structures with a 12-fold orientational order. However, the predicted parameter region is presumably difficult to achieve experimentally. Section VI summarizes the results and discusses the limitations of our approach.

II. THE SYSTEM AND BASIC EVOLUTION EQUATIONS IN OB APPROXIMATION

A fluid layer of depth d and infinite lateral extent is bounded in the vertical z direction by two horizontal plates.

For an incompressible fluid the balance equations for mass, momentum, and energy read

$$\partial_t \vec{u} = -(\vec{u}\cdot\vec{\nabla})\vec{u} + \nu\nabla^2\vec{u} - \frac{1}{\rho_0}\vec{\nabla}\mathrm{p} - g(t)[1-\alpha(T-T_0)]\vec{e}_z, \tag{2.1}$$

$$\partial_t T = -(\vec{u}\cdot\vec{\nabla})T + \kappa\nabla^2 T, \tag{2.2}$$

$$\vec{\nabla}\cdot\vec{u} = 0, \tag{2.3}$$

where $\vec{u}(\vec{r},t)=(u,v,w)$ is the velocity field, $p(\vec{r},t)$ the pressure, and $T(\vec{r},t)$ the temperature field. For the time being, the material parameters, kinematic viscosity ν, thermal expansion coefficient α, and heat diffusivity κ are assumed to be constant. This is the essence of the OB approximation. A thermal drive of the setup is imposed by an external temperature difference ΔT between the covering plates. We indicate heating from above by a negative ΔT. The apparatus is also subjected to a mechanical drive by shaking it in vertical direction. In the comoving frame of reference this gives rise to a time-dependent gravity modulation $g(t)=g_0(1+\varepsilon\ \cos\omega t)$, where ε and ω are the mechanical control parameters.

For weak mechanical and thermal drive, the fluid remains in its rest state $\vec{u}=\vec{0}$, where the pressure p balances the time-dependent gravity field $g(t)$. The temperature profile of this purely conductive state varies linearly according to $T=T_0-z\Delta T/d$, where T_0 denotes a reference temperature in the midplane between the plates.

In order to investigate the nonlinear convective properties it is useful to introduce the deviation θ from the conductive temperature profile. Furthermore we use dimensionless units where length is scaled by d, velocity by κ/d, time by d^2/κ, pressure by $\rho_0\kappa^2/d^2$, and temperature by $\kappa\nu/(\alpha g_0 d^3)$. The pressure in Eq. (2.1) can be eliminated by operating twice with curl, giving

$$\partial_t\nabla^2\vec{u} = \vec{\nabla}\times\vec{\nabla}\times(\vec{u}\cdot\vec{\nabla})\vec{u} + \sigma\frac{g(t)}{g_0}\begin{pmatrix} -\partial_x\partial_z \\ -\partial_y\partial_z \\ \partial_x^2+\partial_y^2 \end{pmatrix}\Theta + \sigma\nabla^4\vec{u}, \tag{2.4}$$

$$\partial_t\Theta = -(\vec{u}\cdot\vec{\nabla})\Theta + Rw + \nabla^2\Theta. \tag{2.5}$$

Here we have introduced two dimensionless numbers, the Rayleigh number $R=(\alpha g_0 d^3\Delta T)/(\nu\kappa)$ measures the thermal drive, while the Prandtl number $\sigma=\nu/\kappa$ characterizes the fluid. The equations of motion are supplemented by the boundary conditions

$$\Theta = 0, \quad w = 0, \quad \partial_z w = 0$$

at

$$z = \pm 1/2, \tag{2.6}$$

corresponding to rigid (i.e., no-slip), perfectly heat conducting plates at the bottom at $z=-1/2$ and the top at $z=1/2$. Note that the equations of motion and boundary conditions are invariant under a reflection at the midplane between the plates. This property is closely related to the OB approximation.

III. LINEAR STABILITY ANALYSIS

In the absence of a mechanical drive, $\varepsilon=0$, the problem is reduced to the classical Rayleigh-Bénard problem [22]. Heating of the device from below gives rise to an unstable density stratification and convection sets in beyond a critical Rayleigh number $R_c=1708$. Due to the up-down symmetry mentioned above, the vertical dependence of the hydrodynamic eigenfunctions is of definite parity (w, θ even and u, v odd).

If the fluid layer is subcritically heated from below or by heating from above, convective motion can also be obtained by applying a simultaneous gravity modulation ($\varepsilon>0$). Gresho and Sani [3] used a Galerkin technique for an approximative treatment of the linear stability problem. We make a similar ansatz for the hydrodynamic fields

$$\begin{aligned} w(x,z,t) &= X(t)e^{ikx}C_1(z), \\ u(x,z,t) &= (i/k)X(t)e^{ikx}\partial_z C_1(z), \\ v(x,z,t) &= 0, \\ \Theta(x,z,t) &= Y(t)e^{ikx}\cos\pi z, \end{aligned} \tag{3.1}$$

where k denotes a wave number in lateral direction and $C_1(z)$ the first Chandrasekhar function [22]. The latter one is more appropriate [23] than the trigonometric functions used in Ref. [3]. Linearizing Eqs. (2.4) and (2.5), inserting Eq. (3.1), and projecting onto the modes leads to a coupled set of ordinary differential equations for the amplitudes $X(t)$ and $Y(t)$,

$$\partial_t X = -h_1\sigma X + h_2\sigma(1+\varepsilon\ \cos\omega t)Y, \tag{3.2}$$

$$\partial_t Y = -h_3 Y + h_4 R X. \tag{3.3}$$

The coefficients h_j are given in Appendix A. By solving Eq. (3.2) for X and inserting the result in Eq. (3.3), the linear stability problem is reduced to the evolution equation of a parametrically driven oscillator (Mathieu oscillator)

$$\ddot{Y} + 2\gamma\dot{Y} + (\delta + a\ \cos\omega t)Y = 0, \tag{3.4}$$

with k-dependent coefficients:

$$2\gamma = k^2 + \pi^2 + \sigma h_1(k), \tag{3.5}$$

$$\delta = \sigma h_1(k)(k^2+\pi^2) - \sigma h_5(k)R, \tag{3.6}$$

$$a = -\sigma h_5(k)\epsilon R. \tag{3.7}$$

The stable (unstable) conductive state at $R<R_c=1708$ ($R>R_c$) corresponds to the stable hanging (unstable inverted) equilibrium position of the oscillator. From the theory of the Mathieu oscillator it is known that a modulation of gravity can both stabilize the unstable rest state and destabilize the stable rest state. It is the latter case which we are dealing with in the following.

To proceed with the linear analysis we invoke the Floquet theorem and write the solutions of Eq. (3.4) in the form

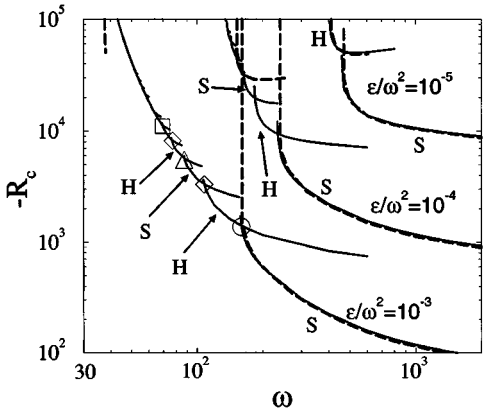

FIG. 1. Critical Rayleigh number as a function of the modulation frequency for fixed modulation amplitudes $\epsilon/\omega^2=10^{-5}$, 10^{-4}, and 10^{-3} and Prandtl number $\sigma=7$. The Rayleigh number is negative since heating is imposed from above. Dashed lines correspond to the results of Clever *et al.* [8]. Capital letters *S* and *H* denote subharmonic and harmonic resonances. A few bicritical points are indicated by symbols.

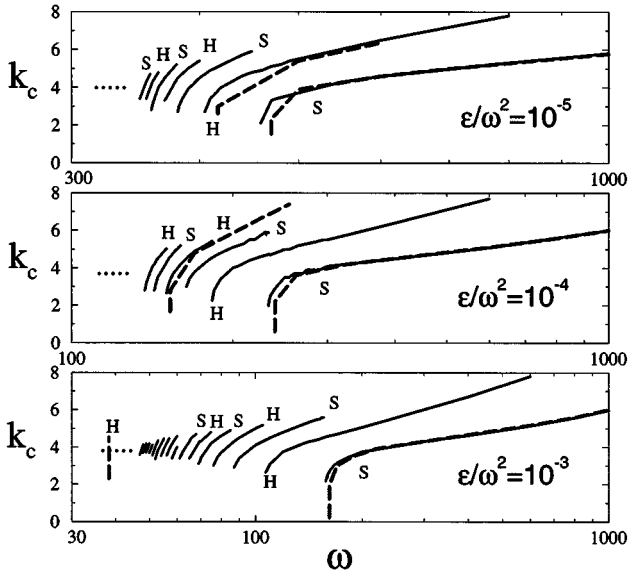

FIG. 2. Critical wave number as a function of the modulation frequency for fixed modulation amplitudes $\epsilon/\omega^2=10^{-5}$, 10^{-4}, and 10^{-3}. See Fig. 1 for further details.

$$Y(t)=e^{\mu t}P(t)=e^{\mu t}\sum_{n=-\infty}^{+\infty}p_n e^{in\omega t}. \tag{3.8}$$

$P(t)$ is a periodic function with the period $2\pi/\omega$ of the drive and μ is the Floquet exponent. As Eq. (3.4) is of second degree, only two Floquet multipliers are possible. With the requirement of a neutrally stable solution (stability boundary), they have to be ± 1 corresponding to the Floquet exponents $\mu=0$ or $\mu=i\omega/2$. This is the reason the Mathieu oscillator resonates either harmonically or subharmonically with respect to the external drive [24]. In the former (latter) case integral (half-integral) multiples of the drive frequency ω contribute to the Fourier spectrum of $Y(t)$. Introducing the Fourier decomposition of $P(t)$ into Eq. (3.4) yields an infinite-dimensional eigenvalue problem (Hill's infinite determinant [24]), with the eigenvalue R depending on the wave number k and the control parameters ε and ω. A minimization of $R(k,\varepsilon,\omega)$ with respect to k yields the threshold $R_c(\varepsilon,\omega)$ and the critical wave number $k_c(\varepsilon,\omega)$. For practical purposes the infinite determinant can be approximated by an appropriate cutoff. We used up to 120 Fourier modes to achieve an accuracy of a few percent. In Fig. 1 the critical Rayleigh number R_c is shown as a function of the modulation frequency ω, while Fig. 2 depicts the corresponding critical wave number $|k_c|$. To compare with earlier work [3,8] we use the shaking elevation ε/ω^2 as a mechanical control parameter instead of the acceleration ε itself. At large frequencies ω the system always responds subharmonically (S), while we observe an alternating sequence of harmonic (H) and subharmonic instabilities towards smaller frequencies. This observation is in partial compliance with the earlier results of Clever *et al.* [8] (dashed lines in Figs. 1 and 2). While their subharmonic branch at high ω agrees well with our findings, their alternating cascade towards smaller ω is only rudimentarily reproduced. We confirmed our calculation within an accuracy of 3.5% with the help of control runs, done with an improved spatial resolution of the eigenfunctions [taking four Galerkin modes in Eq. (3.1) instead of only one]. The instability branches missing in Ref. [8] might be due to an insufficient k resolution in the minimum finder for k_c. In Fig. 3 we explain a typical subharmonic to harmonic transition (open circle in Fig. 1) by means of the neutral curves $R(k)$: For an excitation frequency $\omega=245$ [Fig. 3(a)] the outer left subharmonic tongue provides the absolute minimum and thus determines R_c and k_c^S. As ω is reduced [Fig. 3(b)] this tongue retracts until its minimum reaches the level of the adjacent harmonic tongue. This is the bicritical situation, where the wave number discontinuously jumps from k_c^S to k_c^H (see Fig. 2). During a further reduction of ω [Fig. 3(c)] the harmonic instability preempts the subharmonic one. Eventually the latter one transforms into an isle before disappearing. By reducing ω even further the dominating harmonic tongue also starts retracting until it is preempted by the next adjacent tongue, etc.

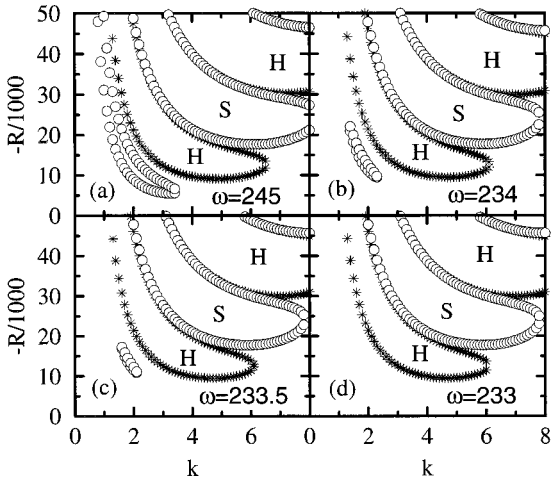

FIG. 3. Bicritical transition (○ in Fig. 1) in the marginal stability chart $R(k)$. From (a) to (d) the forcing frequency ω is reduced.

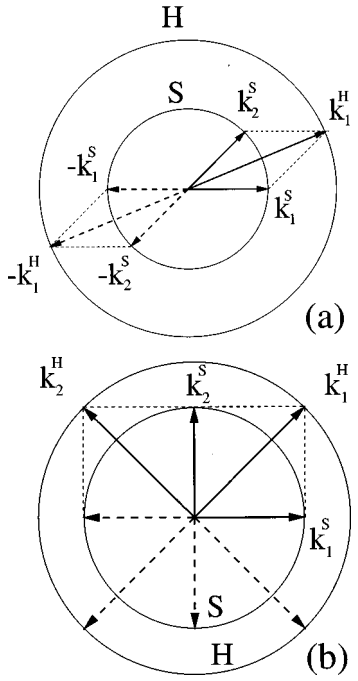

FIG. 4. Triad wave-vector coupling. (a) Two subharmonic modes with wave vectors k_1^S, k_2^S resonate with a harmonic mode of wave vector k_1^H. (b) If the angle between k_1^S and k_2^S is 90° a second harmonic wave vector k_2^H contributes to the resonant energy exchange.

IV. THREE-WAVE-VECTOR RESONANCE AT THE BICRITICALITY

In this section the focus is on the bicritical situations indicated in Fig. 1 by symbols. The idea is that two subharmonic modes with lateral wave vectors k_1^S and k_2^S nonlinearly interact with a harmonic mode k_1^H by virtue of a triad resonance [Fig. 4(a)]. The resonance mechanism is most effective if k_1^S and k_2^S enclose an angle of 90° as a second harmonic wave vector k_2^H can contribute to the coupling [Fig. 4(b)]. Since this interaction mechanism couples subharmonic and harmonic modes we denote it as ''cross'' resonance. The convection pattern driven by the cross resonance depicted in Fig. 4(b) consists of two superimposed sets of squares (45° rotated relative to each other) with respective wave numbers $|k^S|$ and $|k^H|$. The 90° angle between k_1^S and k_2^S requires a wave-number ratio of $k^H/k^S \simeq \sqrt{2}$ at the bicriticality. In Fig. 5 we demonstrate how this ratio can be tuned by varying the driving elevation ε/ω^2. We read off that the desired value of $\sqrt{2}$ is achieved by the open triangle bicriticality (see Fig. 1) at the following control parameters:

$$\epsilon/\omega^2 = 8.3266 \times 10^{-3},$$

$$\omega = 65.6914, \tag{4.1}$$

where $R_c \simeq -925.945$, $k_c^S \simeq 3.03$, and $k_c^H = \sqrt{2} k_c^S \simeq 4.28$ [25]. The cross resonance discussed so far is not the only possible triad wave-vector coupling. We observe that three wave vectors of *equal* length may also resonate if their mutual enclosed angle is 120°. We denote this mechanism, which forces hexagonal structures [19,26,20,21], as *inner* resonance, since only wave vectors of the same length are involved. Note that the inner resonance works only among modes with *harmonic* time dependence, whereas the *subharmonic* symmetry prohibits any inner resonance. Besides testing for an appropriate temporal behavior, the vertical dependence of the modes must also be checked, whether it allows a successful triad interaction. Indeed, the OB approximation turns out to be problematic: As mentioned above, the up-down symmetry of the system implies even (odd) z dependencies of the eigenfunctions $w, \theta(u,v)$. Accordingly, the convective derivative $\vec{u} \cdot \vec{\nabla}$ in the evolution equations is parity inverting and thus the quadratic nonlinearities cannot couple to $\partial_t w$ and $\partial_t \theta$ in Eqs. (2.4). To overcome this difficulty we release the OB approximation and allow a temperature-dependent viscosity

$$\nu(T) = \nu_0[1 - \nu_1(T - T_0)]. \tag{4.2}$$

The advantage of considering the viscosity in favor of the other material parameters is that the evolution equation for θ and thus the basic conductive state remain unchanged. The necessary modifications of the theory are thus restricted to the Navier-Stokes equation, which transforms to [27]

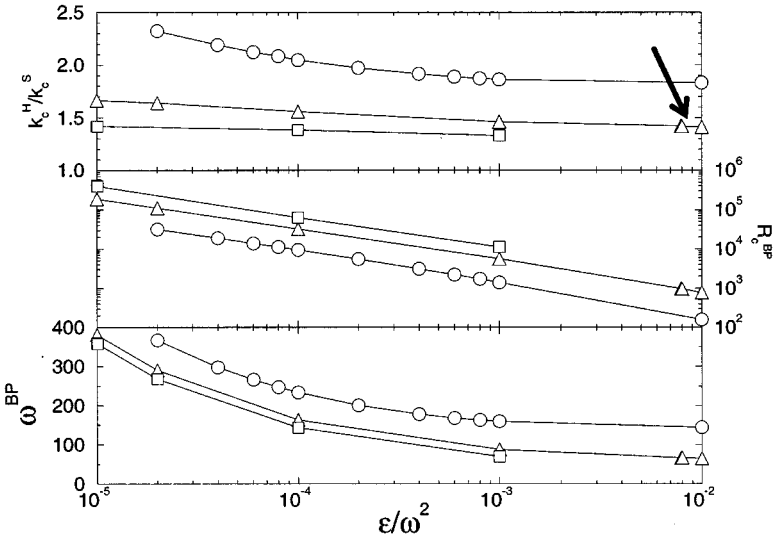

FIG. 5. Wave-number ratio k_c^H/k_c^S, critical Rayleigh number R_c, and modulation frequency ω as a function of the modulation amplitude ε/ω^2 for a few bicritical points shown in Fig. 1. The arrow indicates the parameter value where $k_c^H/k_c^S \simeq \sqrt{2}$. Prandtl number is fixed at $\sigma = 7$.

$$\partial_t u_i = -(\vec{u}\cdot\vec{\nabla})u_i + \sigma_0\nabla^2 u_i - \partial_i p + \sigma_0(1+\epsilon\cos\omega t) \times\Theta\,\delta_{i,3} + \sigma_1\sigma_0 z\nabla^2 u_i + \sigma_1\sigma_0(\partial_z u_i + \partial_i w) - \frac{\sigma_1}{R}\sigma_0\Theta\nabla^2 u_i - \frac{\sigma_1}{R}\sigma_0\vec{\nabla}\Theta\cdot(\vec{\nabla}u_i + \partial_i\vec{u}). \quad (4.3)$$

Here, $\sigma_0 = \nu_0/\kappa$ substitutes the former Prandtl number σ. The supplementary linear and nonlinear terms are weighted by the dimensionless coefficient $\sigma_1 = \nu_1\Delta T$, which quantifies the NOB effects. σ_1 is supposed to be small (e.g., $\sigma_1 \simeq 0.2$ for a water layer subjected to a temperature difference of 10 K). Both the linear and the nonlinear NOB contributions break the up-down symmetry of the system. The linear terms generate perturbations of order σ_1 in the eigenfunctions w and θ, which destroy the even parity of the vertical dependence. A small correction of order σ_1^2 to the critical Rayleigh number R_c results [27]. We want to ignore these small effects in the following discussion.

V. NONLINEAR PATTERN SELECTION

We are interested in convection patterns close to a bicriticality, where modes with different wavelengths compete. In the presence of NOB effects the dominating nonlinear interaction process close above the onset of instability is the triad wave-vector coupling, which appears here in the form of the inner and the cross resonance. Both mechanisms compete as they try to enforce hexagonal and square patterns, respectively. A minimal Galerkin model, which allows the two coupling mechanisms to evolve freely, requires six lateral Fourier modes on each unstable wave-number circle $|k^S|$ and $|k^H|$. We therefore make the ansatz

$$\vec{u} = \vec{\nabla}\times\vec{\nabla}\times\vec{e}_z\left(\sum_{n=1}^{6} X_n^S e^{i\vec{k}_n^S\cdot\vec{r}} + \sum_{n=1}^{6} X_n^H e^{i\vec{k}_n^H\cdot\vec{r}} + \text{c.c.}\right)C_1(z),$$

$$\Theta = \left(\sum_{n=1}^{6} Y_n^S e^{i\vec{k}_n^S\cdot\vec{r}} + \sum_{n=1}^{6} Y_n^H e^{i\vec{k}_n^H\cdot\vec{r}} + \text{c.c.}\right)\cos\,\pi z + Z\,\sin 2\pi z. \quad (5.1)$$

The above representation of the velocity field implies that the vertical component of the vorticity vanishes. For large Prandtl numbers this is a reasonable approximation [21]. The orientation of the lateral wave vectors $\vec{k}_n^S$ and $\vec{k}_n^H$ is shown in Fig. 6. In analogy to the three-mode Lorenz model [28] for convective rolls, we have introduced the mode Z to provide nonlinear saturation. The model ansatz (5.1) gives sufficient freedom for the system to develop a competition between line, square, hexagonal, or quasiperiodic patterns of 12-fold rotational symmetry.

Inserting the ansatz into Eqs. (4.3) and (2.5), and projecting onto the modes, leads to the following system of 25 ordinary evolution equations:

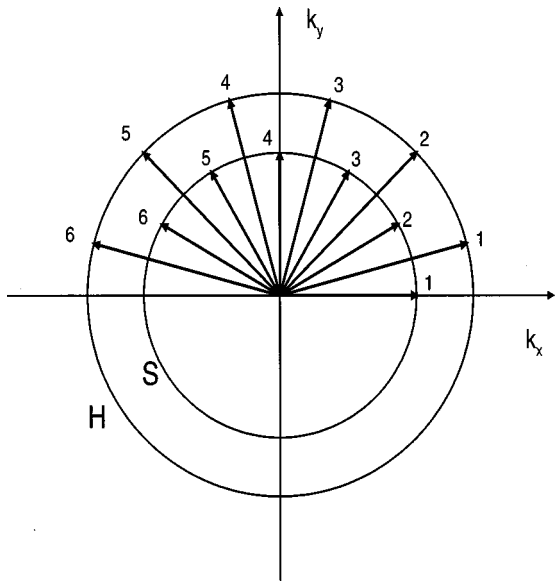

FIG. 6. Lateral wave vectors for a minimum Galerkin model, which allows solutions in the form of lines, squares, hexagons, or quasiperiodic patterns with a 12-fold symmetry axis.

$$\partial_t X_1^S = -j_1\sigma_0 X_1^S + j_5\sigma_0(1+\epsilon\,\cos\,\omega t)Y_1^S + j_2\frac{\sigma_1}{R}\sigma_0(Y_4^{S*}X_2^H + X_5^{H*}Y_4^S) + j_3\frac{\sigma_1}{R}\sigma_0(Y_5^{S*}X_3^S + X_5^{S*}Y_3^S) + j_4\frac{\sigma_1}{R}\sigma_0(Y_5^{H*}X_4^S + X_4^{S*}Y_2^H),$$

$$\partial_t X_1^H = -j_6\sigma_0 X_1^H + j_9\sigma_0(1+\epsilon\,\cos\,\omega t)Y_1^H + j_7\frac{\sigma_1}{R}\sigma_0(Y_6^{S*}X_3^S + X_6^{S*}Y_3^S) + j_8\frac{\sigma_1}{R}\sigma_0(Y_5^{H*}X_3^H + X_5^{H*}Y_3^H),$$

$$\partial_t Y_1^S = j_{10}RX_1^S - j_{11}X_1^S Z - j_{12}Y_1^S,$$

$$\partial_t Y_1^H = j_{10}RX_1^H - j_{11}X_1^H Z - j_{13}Y_1^H,$$

$$\partial_t Z = -j_{14}Z + j_{11}\sum_{i=1}^{6}(Y_i^{S*}X_i^S + Y_i^{H*}X_i^H) + \text{c.c.} \quad (5.2)$$

The remaining 20 equations for $X_i^S, X_i^H, Y_i^S, Y_i^H$ $(i=2,\ldots,6)$ follow by cyclic permutation of the mode indices. The numerical values of the coefficients are given in Appendix B.

To investigate the dynamics and pattern selection of this model we integrated the equations numerically with a fourth-order Runge-Kutta method. Starting from random initial values we found two types of stable patterns: squares or a quasiperiodic structure (Fig. 7). The bifurcation diagram is given in Fig. 8. The primary bifurcation is backwards towards a square convection pattern as shown in Fig. 7(a). As outlined in Fig. 4(b), the structure consists of two sets of squares with wave numbers $|k^S|$ and, respectively, $|k^H|$, rotated by 45° relative to each other. All remaining modes of the model but $Z(t)$ exhibit zero amplitude. The observation of squares indicates that the cross resonance dominates close to the onset

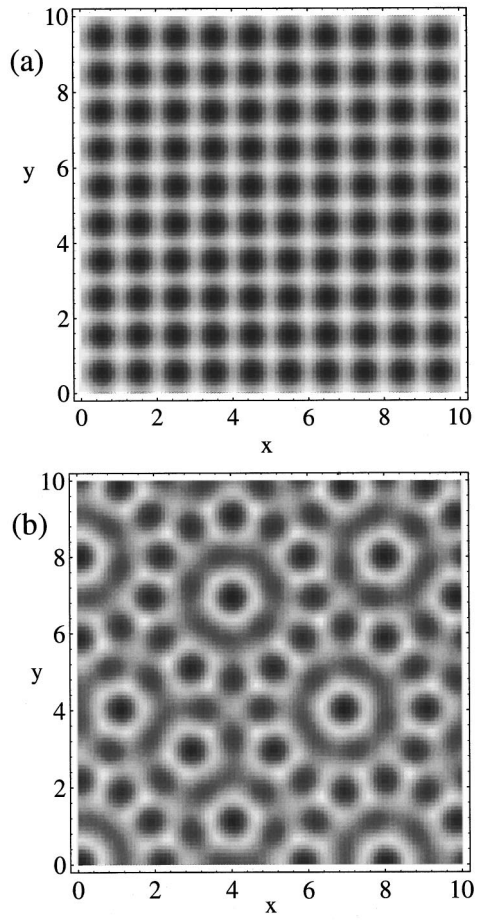

FIG. 7. Density plots of the temperature field as observed in the numerical simulation of the model Eqs. (5.2) with ε and ω according to Eq. (4.1). (a) Stable square pattern. Only the contribution of the subharmonic pattern with $k=k_S$ is visible. The relative amplitude of the squares with $k=k_H$ is only 30%. See Fig. 4(b) for a Fourier decomposition. (b) The quasiperiodic structure.

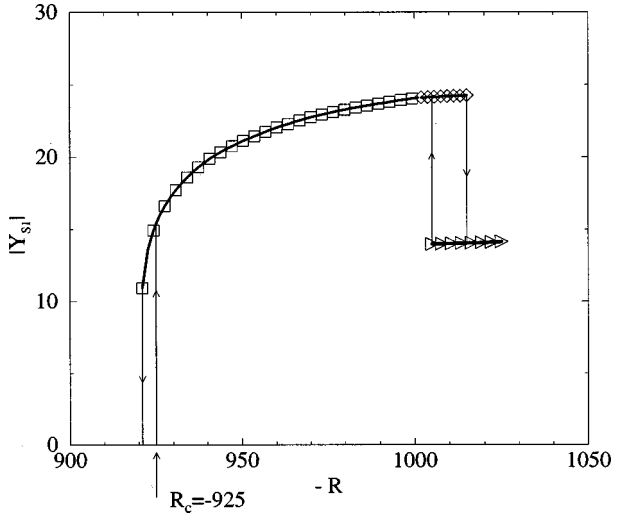

FIG. 8. Bifurcation diagram resulting from integration of the model Eqs. (5.2). Squares (diamonds) indicate stable square patterns with the subharmonic or harmonic time dependence being preserved (broken). Triangles denote stable quasiperiodic patterns as shown in Fig. 7(b).

of the instability. The computer integration of Eqs. (5.2) also provides the time dependences of the excited modes: For the square pattern we find that the subharmonic (harmonic) symmetry of the modes valid at the onset remains preserved in the weakly nonlinear regime.

At $R\approx -1000$ a sudden break of this temporal symmetry occurs: The harmonic (subharmonic) modes X^H, Y^H (X^S, Y^S) receive additional half-integer (integer) frequency contributions in their Fourier sprectra. Due to this bifurcation, the inner resonance among S modes is no longer prohibited, and both resonance mechanisms are able to take full advantage of the nonlinear coupling. As a result we observe at $R>\simeq 1010$ a convective structure, in which *all* modes depicted in Fig. 6 are excited. Figure 7(b) shows a shadowgraph of the correponding temperature mode, which exhibits a 12-fold orientational order. By decreasing the control parameter again we find that the transition between squares and the quasiperiodic patterns is slightly hysteretic.

VI. SUMMARY AND DISCUSSION

In this paper we investigate slightly nonlinear pattern formation in Rayleigh-Bénard convection under gravity modulation. We concentrate on bicritical situations, where a harmonic and a subharmonic instability compete. The critical wave numbers k_c^H and k_c^S, under which the two instabilities occur, can be controlled externally. In the case of non-Oberbeck-Boussinesq fluids (e.g., with a temperature-dependent viscosity) the governing nonlinear interaction process is a three-wave-vector resonance. We distinguish between a cross resonance, coupling harmonic to subharmonic modes, and an inner resonance, where only modes of the same wavelength are involved. While the inner resonance always forces hexagonal structures, the preferred pattern driven by the cross resonance depends on the wave-number ratio $|k_c^H/k_c^S|$. This value can be controlled by varying the amplitude and frequency of the gravity modulation. Here we consider the case $|k_c^H/k_c^S|=\sqrt{2}$ for which the cross resonance favors squares. Our aim is to show how the bicritical situation can be used to force convective structures of nontrivial symmetry.

Our investigation is performed in terms of a Galerkin model. By expanding the spatial dependence of the hydrodynamical fields in an appropriate set of test functions, the Navier-Stokes equations are reduced to a set of 25 ordinary differential equations. This is a generalization of the three-mode Lorenz model [28] for convective rolls. The mode truncation has been chosen such that the cross and inner resonance can freely evolve and compete. Regular convection patterns in the form of rolls, squares, hexagons, as well as quasiperiodic structures are possible solutions of the model. The stability finally depends on the dynamics of the model, which is investigated numerically. It turns out that the cross resonance mechanism prevails close to the onset of the instability and square patterns appear at first. At higher Rayleigh numbers, we observe a secondary hysteretic transition towards quasiperiodic patterns. For this pattern the inner and the cross resonance can take full advantage of the triad wave-vector coupling.

We point out that our model approximation suffers from the drawback of any few-mode Galerkin appoximation: If

some pattern appears to be stable, it is stable in a restricted sense, namely, with respect to ''internal'' perturbations: Only those disturbances which can be built up by the participating Galerkin modes can destabilize a solution. External mechanisms (e.g., long wavelength instabilities like Eckhaus or zigzag) are not covered, because the lateral wave numbers of the participating Galerkin modes is fixed. This is similar to the known three-mode Lorenz model for Bénard convection, which is also unable to explain the Eckhaus instability. So far, we cannot exclude that external mechanisms could destabilize any predicted pattern and prevent its experimental observability.

Another approximation in our model is the use of Galerkin modes with *definite* parity of the z dependencies. As outlined above, this assumption is strictly valid only for OB fluids, where the up-down symmetry of the system holds. In NOB fluids the parity of the eigenfunctions of the stability problem is no longer preserved. In our consideration we have ignored these effects since they are weighted by the small NOB parameter σ_1. A consistent way of taking these effects into account would have doubled the size of our model system.

Finally we mention that not all possible NOB effects have been considered in our model. As a representative example we introduced a temperature dependence of the viscosity, because it was easy to implement even though the selection mechanism discussed here applies to any NOB effect. So far our discussion should be understood as a recipe to generate interesting nonlinear structures in a convection experiment, rather than giving an exact quantitative prediction.

APPENDIX A: COEFFICIENTS IN THE LINEAR EQUATIONS

$$h_1 = -d_1(k)/d_2(k), \tag{A1}$$

$$h_2 = -4\pi k^2\lambda^2/[d_2(k)(\lambda^4-\pi^4)], \tag{A2}$$

$$h_3 = k^2+\pi^2, \tag{A3}$$

$$h_4 = 8\pi\lambda^2/(\lambda^4-\pi^4), \tag{A4}$$

$$h_5 = -(32\pi^2k^2\lambda^4)/[d_2(k)(\lambda^4-\pi^4)^2], \tag{A5}$$

with

$$d_1 = (\lambda^2-k^2)^2c_1+(\lambda^2+k^2)^2c_2-\lambda(k^4+\lambda^4)c_3, \tag{A6}$$

$$d_2 = (\lambda^2-k^2)c_1-(\lambda^2+k^2)c_2+k^2c_3, \tag{A7}$$

$$c_1 = (\lambda+\sinh\lambda)/(2\lambda\ \cosh\lambda/2), \tag{A8}$$

$$c_2 = (\lambda+\sin\lambda)/(2\lambda\ \cos\lambda/2), \tag{A9}$$

$$c_3 = 2\,\frac{\sinh\lambda/2\ \cos\lambda/2+\cosh\lambda/2\ \sin\lambda/2}{\lambda\ \cosh\lambda/2\ \cos\lambda/2}, \tag{A10}$$

$$\lambda = 4.730\ 04. \tag{A11}$$

APPENDIX B: COEFFICIENTS IN THE 25-MODE MODEL

$$\sigma_0 = 7, \tag{B1}$$

$$\sigma_1 = 0.86, \tag{B2}$$

$$j_1 = 37.7371, \tag{B3}$$

$$j_2 = 16.3287, \tag{B4}$$

$$j_3 = 15.1799, \tag{B5}$$

$$j_4 = 9.54\ 917, \tag{B6}$$

$$j_5 = 0.421\ 322, \tag{B7}$$

$$j_6 = 42.0464, \tag{B8}$$

$$j_7 = 22.8824, \tag{B9}$$

$$j_8 = 19.0064, \tag{B10}$$

$$j_9 = 0.590\ 41, \tag{B11}$$

$$j_{10} = 0.9862, \tag{B12}$$

$$j_{11} = 5.0989, \tag{B13}$$

$$j_{12} = 19.0457, \tag{B14}$$

$$j_{13} = 28.2217, \tag{B15}$$

$$j_{14} = 39.478. \tag{B16}$$

[1] For a review see S. H. Davis, Annu. Rev. Fluid Mech. **8**, 57 (1976).
[2] G. J. Venezian, J. Fluid Mech. **35**, 243 (1969).
[3] P. M. Gresho and R. L. Sani, J. Fluid Mech. **40**, 783 (1970).
[4] S. Rosenblat and G. A. Tanaka, Phys. Fluids **14**, 1319 (1971).
[5] G. Ahlers, P. C. Hohenberg, and M. Lücke, Phys. Rev. Lett. **53**, 48 (1983); Phys. Rev. A **32**, 3493 (1984).
[6] P. C. Hohenberg and J. B. Swift, Phys. Rev. A **35**, 3855 (1987).
[7] S. Biringen and L. J. Peltier, Phys. Fluids A **2**, 754 (1990).
[8] R. Clever, G. Schubert, and F. H. Busse, J. Fluid Mech. **253**, 663 (1993).
[9] R. Clever, G. Schubert, and F. H. Busse, Phys. Fluids A **5**, 2430 (1993).
[10] M. C. Cross, P. C. Hohenberg, and M. Lücke, J. Fluid Mech. **136**, 269 (1983).
[11] M. N. Roppo, S. H. Davis, and S. Rosenblat, Phys. Fluids **27**, 796 (1984).
[12] R. G. Finucane and R. E. Kelly, Int. J. Heat Mass Transf. **19**, 71 (1976).
[13] G. Ahlers, P. C. Hohenberg, and M. Lücke, Phys. Rev. A **32**, 3519 (1985).
[14] J. J. Niemela and R. J. Donnelly, Phys. Rev. Lett. **57**, 583 (1986); **59**, 2431 (1987).

[15] C. W. Meyer, D. S. Cannell, G. Ahlers, J. B. Swift, and P. C. Hohenberg, Phys. Rev. Lett. **61**, 947 (1988).
[16] C. W. Meyer, D. S. Cannell, and G. Ahlers, Phys. Rev. A **45**, 8583 (1992).
[17] W. S. Edwards and S. Fauve, J. Fluid Mech. **278**, 123 (1994).
[18] We are considering systems with rotational symmetry in the pattern forming plane. Accordingly, the set of critical wave vectors is always a circle with radius $|k|=k_c$.
[19] E. Palm, J. Fluid Mech. **8**, 183 (1960).
[20] A. Schlüter, D. Lortz, and F. H. Busse, J. Fluid Mech. **23**, 129 (1965).
[21] F. H. Busse, J. Fluid Mech. **30**, 625 (1967), and cited references.
[22] S. Chandraskhar, *Hydrodynamic and Hydromagnetic Stability* (Clarendon, Oxford, 1961).
[23] J. Niederländer, M. Lücke, and M. Kamps, Z. Phys. B **82**, 135 (1991).
[24] A. H. Nayfeh and D. T. Mook, *Nonlinear Oscillations* (Wiley, New York, 1979).
[25] In order to show how to return to dimensional units we give here an example for a thin methanol layer ($d=0.5$ mm, $\kappa=0.107$ mm^2/s, $\alpha=0.0012$/ K, $\nu=0.742$ mm^2/s, $\sigma\simeq 7$): $\omega=65.69\times\kappa/d^2=2\pi\times 4.5$ Hz (forcing frequency), $\varepsilon g_0=8.3\times 10^{-3}\times(65.69)^2\times g_0=35.8 g_0$ (acceleration), and $z_0=\varepsilon/\omega^2 g_0(d^2/\kappa)^2=445$ mm (peak elevation). The critical Rayleigh number of $R_c=-925.945$ corresponds to a temperature difference betweeen the plates of $\Delta T\simeq 44$ K. In view of the high peak elevation and the considerable temperature difference an experimental realization is probably difficult.
[26] L. A. Segel and J. T. Stuart, J. Fluid Mech. **13**, 289 (1962).
[27] E. Palm, T. Ellingsen, and B. Gjevik, J. Fluid Mech. **30**, 651 (1967).
[28] E. N. Lorenz, J. Atmos. Sci. **20**, 130 (1963).